Letters

A Dynamic Wireless Power Transfer System Using DC-Controlled Variable Inductor for Segment Transmitter Automatic Switching

Zeheng Zhang, *Student Member, IEEE*, Zheng Li, Xiaojun Zhang, Bin Yang, *Student Member, IEEE*, Zhengyou He, *Senior Member, IEEE*, Ruikun Mai, *Senior Member, IEEE*, and Yang Chen, *Senior Member, IEEE*

***Abstract*—Segmented transmitter coils are commonly employed in dynamic wireless power transfer, and automatic switching is a preferred function to limit the transmitter current. This letter proposes a method for segment transmitter automatic switching utilizing a dc-controlled variable inductor (DCCVI), where the dc current can change the ac side's self-inductance. When the coils are decoupled, the dc current is small, so the inductance of the DCCVI is relatively large, leading to the suppression of the transmitter current. When the coils meet certain coupling conditions, the dc current becomes large, leading to a significant reduction in the ac inductance of the DCCVI, resulting in higher transmission power, thereby enabling segment transmitter automatic switching. The proposed method is straightforward and does not need additional position feedback. The experimental results demonstrate that the proposed system can automatically limit the coil current within the range of [0, 0.15] and achieve higher power transmission with higher efficiency within the coupling range of [0.165, 0.3].**

***Index Terms*—Automatic switching, dynamic wireless power transfer (DWPT), variable inductor.**

I. Introduction

DYNAMIC wireless power transfer (DWPT) offers increased flexibility in power transmission by reducing the need for prolonged stationary charging [1], [2], [3]. Segmented transmitter coils are recommended for DWPT due to their construction complexity and high power losses. These coils can be selectively coupled to mobile receiving coils. However, to limit the current and transmitted power of the transmitter coil

Manuscript received 22 April 2024; revised 25 May 2024 and 25 June 2024; accepted 29 June 2024. Date of publication 10 July 2024; date of current version 12 December 2024. This work was supported in part by the National Natural Science Foundation of China under Grant 52207226, in part by the Sichuan Science and Technology Program under Grant 2023NSFSC0819, in part by the Fundamental Research Funds for the Central Universities under Grant 2682024CX025, and in part by the Sichuan Nature and Science Foundation Innovation Research Group Project under Grant 2023NSFSC1975. *(Corresponding author: Yang Chen.)*

The authors are with the Key Laboratory of Magnetic Suspension Technology and Maglev Vehicle, Ministry of Education, Chengdu 611756, China, and also with the School of Electrical Engineering, Southwest Jiaotong University, Chengdu 611756, China (e-mail: hengs@my.swjtu.edu.cn; li_zheng@my.swjtu.edu.cn; yiquebkx@my.swjtu.edu.cn; yb@my.swjtu.edu.cn; hezy@home.swjtu.edu.cn; mairk@swjtu.edu.cn; yangchen@swjtu.edu.cn).

Color versions of one or more figures in this article are available at https://doi.org/10.1109/TPEL.2024.3426100.

Digital Object Identifier 10.1109/TPEL.2024.3426100

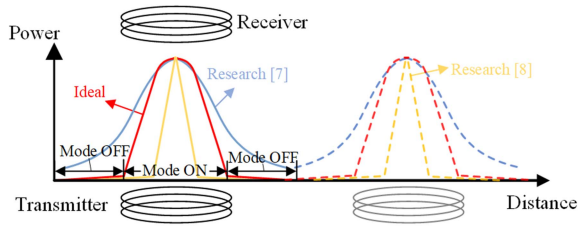

Fig. 1. Transfer power curves of automatic switching methods in [7] and [8].

[4], receiver position feedback and decoupling coil methods are necessary. Some researchers [5], [6] have proposed methods involving sensors to detect the receiver's position and control the transmitter's current. However, such methods require additional control circuits and sensors. To alleviate the complicated control methods, Lee et al. [7] introduced a current attenuation technique devoid of explicit control requisites. However, the current attenuation of this method is slow in the process of coil decoupling, termed "Mode OFF," rendering power losses and electromagnetic radiation. In addition, Dayerizadeh et al. [8] proposed a new method with superior field-focusing ability to reduce the transmitter current rapidly, but that greatly decreases the coupling range for power transmission (this interval is named "Mode ON"). Therefore, the "ideal" curve (see Fig. 1) is better than that in [7] and [8]. Specifically, the ideal scenario is to have a larger coupling range during the "Mode ON" period and a smaller transmitter current during the "Mode OFF" period.

This letter proposes a DWPT system that addresses the aforementioned issues for segment transmitter autoswitching. The contributions are highlighted and summarized as follows.

1) This letter proposes a DWPT system by introducing a dual-E-type dc-controlled variable inductor (DCCVI) for segment transmitter automatic switching. The inductor's ac bias and dc bias are connected in series to the inverter's ac output and dc input, respectively. The dc input current can modify the ac side's self-inductance and obviates the need for auxiliary circuits and detection mechanisms, realizing the automatic adjustment of the transmitter current with the change of coupling coefficient.

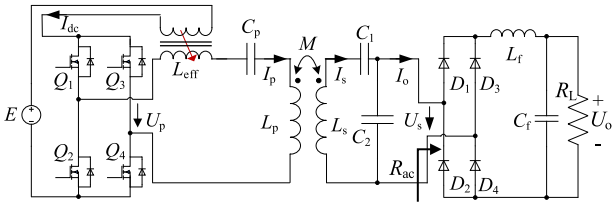

Fig. 2. Proposed DWPT topology with the dual-E-type DC-controlled variable inductor.

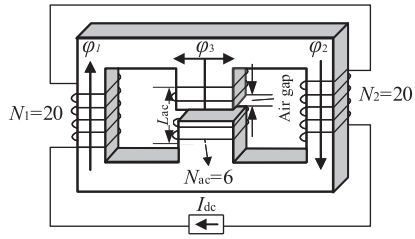

Fig. 3. Diagram of the DCCVI.

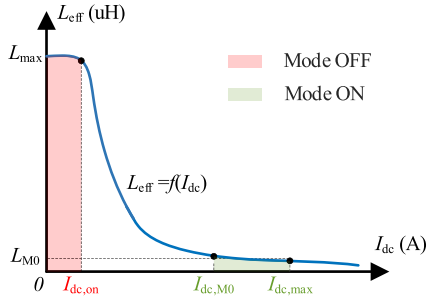

Fig. 4. L_{eff}–I_{dc} curves of the DCCVI.

2) This letter delineates the coil coupling process into two distinct phases: "Mode ON" and "Mode OFF." An innovative parametric design method is proposed to enlarge the coupling range during the "Mode ON" period compared to the prior work, providing a larger interval to transmit power. In addition, the proposed method accelerates the current attenuation speed. It decreases the transmitter current during the "Mode OFF" period compared with the traditional method, reducing the electromagnetic radiation and power loss of the transmitter.

The rest of this letter is organized as follows. In Section II, a DWPT system with a dual-E-type DCCVI is systematically analyzed. Experimental results are provided in Section III to validate the proposed method. Finally, Section IV concludes this letter.

II. Theoretical Analysis

A. Proposed System

The proposed DWPT system employs a series–series parallel topology, as illustrated in Fig. 2, where the DCCVI enables automatic switching. U_p (U_s) is the input (output) voltage of the system, I_p (I_s) denotes the coil current of the transmitter (receiver), I_o is the input current of the rectifier, and R_L indicates the dc load. L_p and C_p are the primary coil and the compensation capacitor, respectively, while L_{eff} is the self-inductance of the DCCVI, which is connected in series with the transmitter. The dc side of the DCCVI is connected in series with the inverter dc input. I_{dc} represents the dc-side current of the DCCVI, which also serves as the dc input current of the system. Notably, L_{eff} can vary with the dc current I_{dc} [9].

The relationship between the input dc voltage E and U_p is expressed as

$$E = \sqrt{2}\pi U_p/4. \tag{1}$$

The secondary coil L_s and compensation capacitors C_1 and C_2 form a receiver with reflective reactance and meet the requirements of [7]

$$\begin{cases} C_1 = \frac{n}{n-1}C \\ C_2 = nC \end{cases} \tag{2}$$

where n is defined as the *tapping coefficient*, and C satisfies [10]

$$\omega = \frac{1}{\sqrt{L_s C}}. \tag{3}$$

The impedance reflected to the transmitter coil is

$$Z_{\text{reflected}} = \frac{\omega M^2}{L_s}(Qn^2 - jn) \tag{4}$$

where $M = k\sqrt{L_p L_s}$ represents the mutual inductance. $Q = R_{\text{eq}}/\omega L_s$ is the quality factor of the receiver.

The input impedance of the system is split into real and imaginary parts, namely

$$Z_{\text{in}} = \frac{\omega M^2}{L_s}Qn^2 + j\left(\Delta Y - \frac{\omega M^2}{L_s}n\right) \tag{5}$$

where ΔY is the transmitter impedance, i.e.,

$$\Delta Y = \omega \cdot L_p - 1/\omega \cdot C_p + \omega \cdot L_{\text{eff}}. \tag{6}$$

Then, the output power can be expressed as

$$P = \text{Re}(U_p^2/Z_{\text{in}}) = \frac{QX_{Ls}n^2M^2U_p^2}{\omega^2Q^2n^4M^4 + (X_{Ls}\Delta Y/\omega - n\omega M^2)^2} \tag{7}$$

where $X_{Ls} = \omega L_s$. Based on (7), it is found that the output power curve changes in the opposite direction to the variation of ΔY. Thus, adjusting the variable L_{eff} in ΔY can modify the output power curve.

B. Design of the DCCVI

The DCCVI [11] is based on a dual-E-core structure (see Fig. 3), with the main inductor (ac) wound around the center arm and the symmetrical bias coil (dc) wound around the two side arms of the core. The side arm winding is connected in series with opposite polarity, effectively reducing the self-inductance value of the central arm by increasing the dc current in the sidewall winding (see Fig. 4).

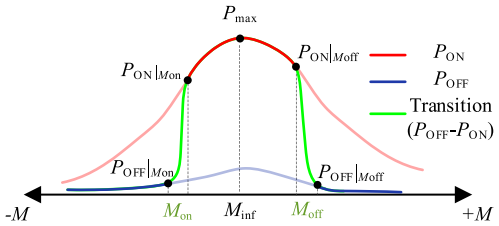

Fig. 5. Transmission power curve with the mutual inductance.

When there is no dc input current, L_{eff} has the maximum value

$$L_{\max} = \frac{N_{\text{ac}}^2}{\ell_e/\mu A_e + g/\mu_0 A_e} \tag{8}$$

where N_{ac} is the number of turns in the central arm, and A_e, l_e, and g represent the effective magnetic cross section, the effective magnetic path length, and the air gap, respectively. μ and μ_0 are the magnetic permeabilities of the core material and vacuum, respectively. To ensure that L_{eff} achieves significant self-inductance attenuation, the external path of the magnetic core must reach saturation, and for the maximum designed dc control current, the number of turns of the control winding can be estimated, i.e.,

$$N_{\text{dc}} = \frac{B_{\text{sat}}\ell_{\text{ext}}}{\mu I_{\text{dc,on}}} \tag{9}$$

where B_{sat}, l_{ext}, and $I_{\text{dc,on}}$ separately represent the saturation magnetic flux density, the external path length of the core, and the maximum value of the dc control current from which the minimum inductance value is obtained.

According to the characteristics that the self-inductance of the transformer inductor varies with the dc current, the L_{eff}–I_{dc} curves of the DCCVI can be roughly outlined in Fig. 4. It can be observed that when the dc current $I_{\text{dc}} < I_{\text{dc,on}}$, L_{eff} maintains a large value, denoted as $L_{\max}$, indicating that the DCCVI operates in the "Mode OFF" period. Conversely, when $I_{\text{dc}} > I_{\text{dc,M0}}$, L_{eff} remains roughly constant at L_{M0}, indicating operation in the "Mode ON" period. Therefore, L_{eff} can be described as

$$\begin{cases} L_{\text{eff}} = L_{\max}, 0 < I_{\text{dc,on}} \\ L_{\text{eff}} = L_{\text{M0}}, I_{\text{dc,M0}} < I_{\text{dc}} < I_{\text{dc,max}} \end{cases}. \tag{10}$$

C. Analysis of the Autoswitching

The entire operational process is illustrated in Fig. 5. When the coil is nearly decoupled ($M = 0$), the system operates in "Mode OFF," and the dc input current can be expressed as

$$I_{\text{dc,off}} = \frac{2\sqrt{2}}{\pi} \cdot \text{Re}(U_p/j(\omega \cdot L_p - 1/\omega \cdot C_p + \omega \cdot L_{\max})). \tag{11}$$

Due to the large reactive component $\omega L_{\max}$, the current of the transmitter is well suppressed, where the output power curve is P_{OFF}. As coupling increases, the dc input current gradually rises, and when the mutual inductance reaches M_{on}, the dc input current is denoted as $I_{\text{dc,on}}$, i.e., [12]

$$I_{\text{dc,on}} = \frac{2\sqrt{2}}{\pi} \cdot \text{Re}\left(U_p/\left(\frac{\omega M_{\text{on}}^2}{L_s}\left(Qn^2 - jn\right) + j\Delta Y\right)\right) \tag{12}$$

where the value of L_{eff} in ΔY is $L_{\max}$. Subsequently, L_{eff} drops and I_{dc} increases rapidly. The system swiftly transitions from "Mode OFF" to "Mode ON," and the output power turns from P_{OFF} into P_{ON}. In "Mode ON," the system operates with a large operating current. The reflected reactance of the receiver neutralizes the reactive component in the coupled transmitter branch. When the coil is fully aligned ($M = M_0$), the total impedance of the transmitter branch should be nearly pure resistance, i.e.,

$$\frac{\omega M_0^2}{L_s} n = \omega L_p - \frac{1}{\omega C_p} + \omega L_{\text{M0}}. \tag{13}$$

Solving (13), C_p can be calculated as

$$C_p = -\frac{L_s}{\omega^2\left(nM_0^2 - (L_p + L_{\text{M0}})L_s\right)}. \tag{14}$$

Then, the dc input current is $I_{\text{dc,M0}}$, i.e.,

$$I_{\text{dc,M0}} = \frac{2\sqrt{2}}{\pi} \cdot \text{Re}\left(U_p/\frac{\omega M_0^2}{L_s} Qn^2\right). \tag{15}$$

When mutual inductance is reduced to M_{off}, the dc current is approximately reduced to $I_{\text{dc,M0}}$, i.e.,

$$I_{\text{dc,M0}} = \frac{2\sqrt{2}}{\pi} \cdot \text{Re}\left(U_p/\frac{\omega \cdot M_{\text{off}}^2}{L_s}(Qn^2 + jn)\right). \tag{16}$$

During this period, the system becomes unstable and automatically reverts to "Mode OFF," causing the power curve to return to P_{OFF}. Thus, the power function can be expressed as

$$\begin{cases} P_{\text{OFF}}, & [0, M_{\text{on}}) \text{ and } [0, M_{\text{off}}) \\ P_{\text{ON}}, & [M_{\text{on}}, M_{\text{off}}] \end{cases} \tag{17}$$

where $P_{\max}$ is the maximum output power during the system operation, and it occurs at $\partial P_{\text{ON}}/M_{\text{inf}} = 0$; the mutual inductance at the maximum power point is obtained as

$$M_{\text{inf}} = \sqrt[4]{\frac{\omega^2 L_s^2 M_0^4}{\omega^2 L_s^2 + R_{\text{eq}}^2 n^2}}. \tag{18}$$

We define $\Delta M = M_{\max}/M_{\min}$ to quantify the enhancement of the coupling range in the proposed system, where $M_{\min}$ is the minimum value of M_{on} and M_{off}, and $M_{\max}$ is the maximum mutual inductance during the system operation, i.e., M_0. When $\Delta M = 1$, $M_{\max}$ and $M_{\min}$ coincide, which means that the system can only achieve higher power at one point. As ΔM increases, the coupling range in which the system attains higher power also expands. Combined with (15) and (16), ΔM can be derived as

$$\Delta M = \frac{\sqrt{Q^2 \cdot n^2 + 1}}{Q \cdot n}. \tag{19}$$

Fig. 6 shows the values of ΔM with different Q and n. It is evident that ΔM monotonically decreases with the increase of n and Q. Thus, reducing n and Q is necessary to achieve a larger coupling range. Unfortunately, increasing ΔM will reduce system efficiency and current gain G (the transmitter current ratio of coil alignment to coil decoupling) [7].

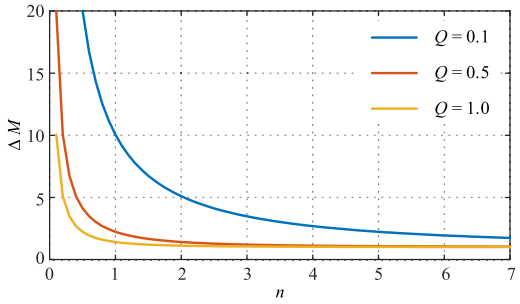

Fig. 6. Values of ΔM with different Q and n.

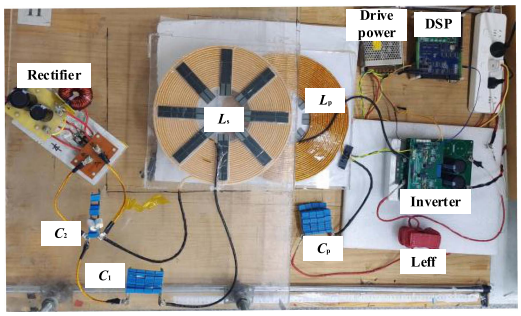

Fig. 7. Experimental prototype.

TABLE I
SYSTEM SPECIFICATION AND PARAMETER DESIGN VALUES

Parameter	Value	Parameter	Value
f	85 kHz	n	3.8
core	EE70	g	0
N_{ac}	6	N_{dc}	40
L_p	145.43 μH	C_1	37.29 nF
C_p	31.69 nF	C_2	16.98 nF
L_s	137.43 μH	L_{max}	196.5 μH
M_0	43.05 μH	L_{M0}	11.27 μH
$I_{dc,on}$	0.5A	R_L	18 Ω

In summary, the selection of parameters must aim to minimize the fluctuation in transmission power while satisfying the prerequisite for system automatic switching.

III. Experimental Validation

A. Experimental Results

To verify the feasibility of the proposed method, an experimental prototype was built, as shown in Fig. 7. The system parameters are shown in Table I.

The steady-state waveforms of the output voltage/current of the transmitter and the input voltage/current of the receiver under different coupling conditions are given in Fig. 8.

In Fig. 8(a) and (b), the peak currents of I_p under decoupled and alignment conditions are 1.9 and 5.8 A, respectively. It shows a current gain of approximately 3.05, demonstrating the effective primary current containment. In Fig. 8(a), the current of the transmitter branch lags behind the voltage by nearly 90°, while the voltage and current are nearly in the zero phase, as shown in Fig. 8(b). Fig. 8(c) displays the steady-state waveform at maximum output power during operation, showing that the

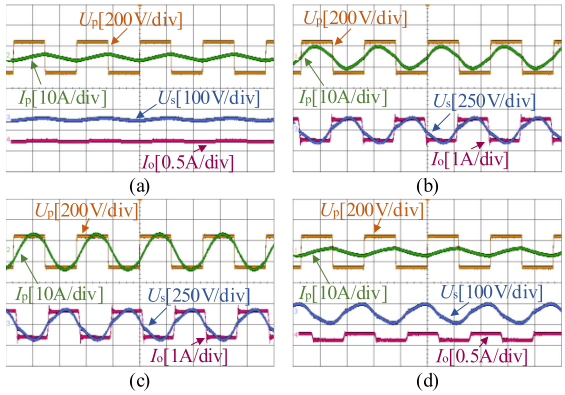

Fig. 8. Experimental waveforms of U_p, I_p, U_s, and I_o. (a) $M = 0$, (b) $M = M_0$, and (c) $M = M_{inf}$ in the proposed system. (d) $M = M_{off}$ (M_{on}) in the proposed system.

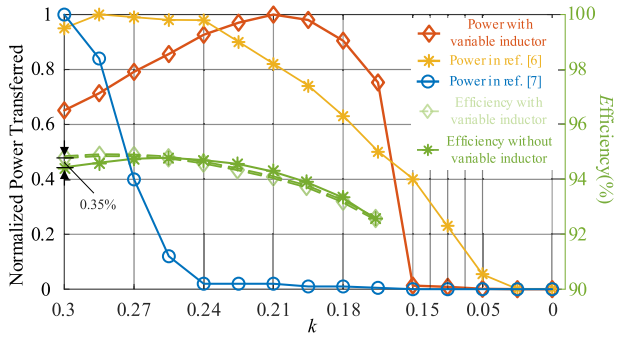

Fig. 9. Normalized transfer power and efficiency of different methods.

current slightly leads the voltage waveform, and the peak voltage and current of the receiver branch are maximum. In Fig. 8(d), the current still lags behind the voltage and remains at a low level. This finding indicates that the transmitter branch contains a large reactive power component due to the DCCVI at $M = M_{on}$ and $M = M_{off}$, achieving a good current suppression effect.

To compare the proposed system with [7] and [8], the transferred power as the coupling variations was measured, as shown in Fig. 9.

From Fig. 9, it can be observed that the proposed system maintains transmission power above 60% in the coupling interval [0.165, 0.3], peaking when the coupling coefficient is $k = 0.21$; the reason why the maximum power point does not occur at the maximum mutual inductance (M_0) [7] is that the mutual inductance (M_{inf}) at the maximum power cannot equal the maximum mutual inductance (M_0) with alignment unless R_{eq} and n in (18) can be 0. However, in the system of [8], the effective coupling range is only [0.28, 0.3]. For the proposed method, the transmitter coil's current decreases rapidly, when the coupling coefficient k is below 0.165, resulting in a reduction of output power. A notable observation is that compared to the method in [7], the proposed system significantly suppresses the transmitter coil's current within the coupling range [0, 0.15]. Based on the experimental results, the calculated values of ΔM for the proposed system and literature [7] and [8] are 1.82, 1.66, and 1.06. It indicates that the proposed system widens the coupling range of the system during the "Mode ON" period. As shown in Fig. 9, the disparity in efficiency between configurations with and without

TABLE II
COMPARISON WITH OTHER METHODS REPORTED IN THE LITERATURE

Literature	[13]	[7]	[8]	This work
Operating frequency	85 kHz	100 kHz	88 kHz	85 kHz
Current gain (G)	11	2.69	14.2	3.05
ΔM	<2	1.62	1.06	1.82
Coupling range	0–0.72	0–0.224	0–0.2	0–0.3
Efficiency	88.4%–96.7%	77.8%–94.5%	81.6%	92.6%–94.7%

The ΔM is defined as "maximum (alignment) mutual inductance – the mutual inductance at 60% power transmission".

the variable inductor is negligible, measuring a mere 0.35%. For the proposed system, the efficiency remains consistently above 92%, and the efficiency increases slightly with the decrease of the coupling coefficient. When the coupling coefficient reaches 0.255, the system efficiency reaches the maximum of 94.7%, and then, the efficiency begins to decline. However, for the system without the variable inductor, the coupling coefficient remains above 94.7% after 0.27, which is higher than that of the system with the variable inductor. As the coupling coefficient continues to decrease, the efficiency also decreases and is lower than that of the system with the variable inductor. Thus, based on empirical findings, the integration of the variable inductor exhibits no discernible impact on system efficiency.

B. Discussion and Comparison

To show the superiority of the proposed method with better segment transmitter automatic switching ability, the performance of the proposed approach is compared with that of other methods, as presented in Table II.

The approach delineated in [13] exhibits a large current gain (G). However, this method requires the system to operate under the tight coupling condition of the coupling coefficient of 0.72, which is not widely used in contemporary wireless power transfer systems. Compared with the method in [7], its coupling range conforms to commonly used designs, yet its G, ΔM, and average efficiency are all lower than those of the proposed system. The proposed method has larger ΔM and efficiency than those of the method in [8] even though G is smaller. Especially, ΔM in [8] is very close to 1, which means that the method can only transfer power with coil alignment.

In summary, the proposed system can automatically switch its operating mode in response to changes in different coupling conditions. The major contribution of this letter is to achieve segment transmitter automatic switching without detection or control. In our future work, we will consider realizing stable output. For example, designing the coil interval, size, structure (shape changes [14], increased dimensions [15]), and coil combination (double-D quadrature coils [16]) can mitigate the fluctuation of the output power. In addition, some control strategies [17], such as dc–dc control, etc., may need to further suppress the fluctuation.

IV. CONCLUSION

This letter proposes a DWPT system that utilizes a dual-E-type DCCVI to realize automatic switching. In this system, the DCCVI is connected with the transmitter in series, whose value can be affected by the dc input current. By varying the values of the DCCVI based on changes in receiver position, the power curve of the system can be altered. This allows for the suppression of the coil current of the transmitter when the coil is decoupled, without requiring any additional position detection. Furthermore, in conjunction with the design of reflective impedances n and Q, the coupling range of the "Mode ON" is improved. The results validate that the proposed system exhibits a good ability for field focusing and segment transmitter automatic switching. In future work, achieving stable output power will be considered.

REFERENCES

[1] V. Cirimele, M. Diana, F. Freschi, and M. Mitolo, "Inductive power transfer for automotive applications: State-of-the-art and future trends," *IEEE Trans. Ind. Appl.*, vol. 54, no. 5, pp. 4069–4079, Sep./Oct. 2018.

[2] T. Fujita, T. Yasuda, and H. Akagi, "A dynamic wireless power transfer system applicable to a stationary system," *IEEE Trans. Ind. Appl.*, vol. 53, no. 4, pp. 3748–3757, Jul./Aug. 2017.

[3] S. Lukic and Z. Pantic, "Cutting the cord: Static and dynamic inductive wireless charging of electric vehicles," *IEEE Electrific.. Mag.*, vol. 1, no. 1, pp. 57–64, Sep. 2013.

[4] *Wireless Power Transfer For Light-Duty Plug-In Electric Vehicles and Alignment Methodology*, SAE Standard J2954, 2016.

[5] S. Choi, J. Huh, W. Y. Lee, S.W. Lee, and C. T. Rim, "New cross-segmented power supply rails for roadway-powered electric vehicles," *IEEE Trans. Power Electron.*, vol. 28, no. 12, pp. 5832–5841, Dec. 2013.

[6] S. Y. R. Hui and W. W. C. Ho, "A new generation of universal contactless battery charging platform for portable consumer electronic equipment," *IEEE Trans. Power Electron.*, vol. 20, no. 3, pp. 620–627, May 2005.

[7] K. Lee, Z. Pantic, and S. M. Lukic, "Reflexive field containment in dynamic inductive power transfer systems," *IEEE Trans. Power Electron.*, vol. 29, no. 9, pp. 4592–4602, Sep. 2014.

[8] A. Dayerizadeh, H. Feng, and S. M. Lukic, "Dynamic wireless charging: Reflexive field containment using saturable inductors," *IEEE Trans. Ind. Appl.*, vol. 56, no. 2, pp. 1784–1792, Mar./Apr. 2020.

[9] D. Medini and S. Ben-Yaakov, "A current-controlled variable-inductor for high frequency resonant power circuits," in *Proc. IEEE Appl.. Power Electron. Conf. Expo.*, 1994. pp. 219–225.

[10] C. Cai et al., "Multistate voltage balancing of UAV's cell string: A reconfigurable WPT-based multiport hybrid charging approach," *IEEE Trans. Ind. Electron.*, early access, Jul. 4 2024, doi: 10.1109/TIE.2024.3401190.

[11] M. S. PerdigÃo, J. M. Alonso, M. A. D. Costa, and E. S. Saraiva, "Using magnetic regulators for the optimization of universal ballasts," *IEEE Trans. Power Electron.*, vol. 23, no. 6, pp. 3126–3134, Nov. 2008.

[12] Y. Chen et al., "A clamp circuit-based inductive power transfer system with reconfigurable rectifier tolerating extensive coupling variations," *IEEE Trans. Power Electron.*, vol. 39, no. 2, pp. 1942–1946, Feb. 2024.

[13] S. Y. Jeong, J. H. Park, G. P. Hong, and C. T. Rim, "Automatic current control by self-inductance variation for dynamic wireless EV charging," in *Proc. IEEE PELS Workshop Emerg. Technol., Wireless Power Transfer*, 2018, pp. 1–5.

[14] K. Aditya, V. K. Sood, and S. S. Williamson, "Magnetic characterization of unsymmetrical coil pairs using Archimedean spirals for wider misalignment tolerance in IPT systems," *IEEE Trans. Transp. Electrific.*, vol. 3, no. 2, pp. 454–463, Jun. 2017.

[15] C. Zheng, H. Ma, J.-S. Lai, and L. Zhang, "Design considerations to reduce gap variation and misalignment effects for the inductive power transfer system," *IEEE Trans. Power Electron.*, vol. 30, no. 11, pp. 6108–6119, Nov. 2015.

[16] Y. Li et al., "A new coil structure and its optimization design with constant output voltage and constant output current for electric vehicle dynamic wireless charging," *IEEE Trans. Ind. Informat.*, vol. 15, no. 9, pp. 5244–5256, Sep. 2019.

[17] Z. Li, C. Zhu, J. Jiang, K. Song, and G. Wei, "A 3-kW wireless power transfer system for sightseeing car supercapacitor charge," *IEEE Trans. Power Electron.*, vol. 32, no. 5, pp. 3301–3316, May 2017.